Desalination and Water Treatment
www.deswater.com

doi: 10.1080/19443994.2015.1108428

57 (2016) 23257–23265
October

Taylor & Francis
Taylor & Francis Group

High-performance ultrafiltration mixed-matrix membranes based on cellulose acetate and nanohydroxyapatite

Gabriela Ciobanu[a,*], Octavian Ciobanu[b]

[a]*Faculty of Chemical Engineering and Environmental Protection, "Gheorghe Asachi" Technical University of Iasi, Prof. Dr. Docent Dimitrie Mangeron Rd., no. 63, 700050 Iasi, Romania, Tel. +40 232232357; Fax: +40 232271311; email: gciobanu03@yahoo.co.uk*
[b]*Faculty of Medical Bioengineering, "Grigore T. Popa" University of Medicine and Pharmacy, Universitatii Str., no. 16, 700115 Iasi, Romania*

Received 30 March 2015; Accepted 6 October 2015

ABSTRACT

The asymmetric cellulose acetate mixed-matrix membrane (MMM) filled with nanohydroxyapatite was prepared by a modified phase inversion method. To prevent the agglomeration of the hydroxyapatite nanocrystals and to obtain ultrafiltration composite membranes, a surfactant (12-hydroxystearic acid) was used. The hydroxyapatite nanopowder was dispersed in acetone-dissolved 12-hydroxystearic acid and then mixed homogeneously with acetone-dissolved cellulose acetate (CA). The process of addition of hydroxyapatite nanosuspension to CA solution resulted in asymmetric composite membranes with higher pure water flux and superior NaCl rejection in comparison to the CA membrane. The best performing composite membrane, the CHM-30 sample, shows a retention of 99.1% and a high water permeability of 34.96 L/m^2 h bar. The results showed that the nanohydroxyapatite—cellulose acetate MMMs can be used in ultrafiltration applications.

Keywords: Mixed-matrix membrane; Cellulose acetate; Hydroxyapatite; Surfactant; Ultrafiltration

1. Introduction

In the last years, many researches have been dedicated to the possibility of obtaining composite materials used for various purposes, such as membrane separation processes for liquid and gaseous mixtures: gas separation, reverse osmosis, pervaporation, nanofiltration, ultrafiltration, and microfiltration [1].

In the membrane separation processes, the polymer–inorganic composites present interesting properties because they possess characteristics of both organic and inorganic ones such as good permeability, selectivity, mechanical strength, and thermal and chemical stability [2].

The incorporation of various kinds of inorganic particles into the polymeric membranes induces the formation of the composite or hybrid membranes that are referred to as mixed-matrix membranes (MMMs) [3]. A special class of MMMs includes nanocomposite membranes where the inorganic filler is a nanomaterial in a size range of 1–100 nm [4]. The presence of

*Corresponding author.

Presented at EuroMed 2015: Desalination for Clean Water and Energy Palermo, Italy, 10–14 May 2015. Organized by the European Desalination Society

finely dispersed inorganic nanoparticles in the polymeric matrix has been proved to be very useful in improving the membrane properties and performances (antifouling, permeation, thermal stabilities, and mechanical properties) for a wide spectrum of processes ranging from gas separation and pervaporation to nanofiltration and ultrafiltration [5].

In recent years, some inorganic nanoparticles (zeolites, silica, carbon nanotube, metal nanopowder, etc.) have been introduced as fillers into the polymeric matrix (polyurethane, polysulfone, cellulose acetate (CA), polyacrylonitrile, polyimide, etc.) to improve the permeation flux or selectivity of the membranes [6–12].

Among the polymeric materials, the CA is used in a large extent in the preparation of the ultra- and nanofiltration membranes for many gas or liquid separation applications due to its good biocompatibility, good toughness, and low price [13–16]. However, the dense skin layer along with low porosity of substructure of the prepared membranes results in a low flux of the CA membranes [17]. Many researchers have been trying to improve the properties of the CA membranes by changing and mixing the solvents in the membrane casting solution, by varying the temperature of coagulation bath or by using different types of additives or pore-forming agents, such as surfactants [17–20].

Recently, composite materials based on calcium phosphate have attracted much attention. The hydroxyapatite (HA), $Ca_{10}(PO_4)_6(OH)_2$, is a calcium phosphate ceramic with important applications in the fields of medicine and chemistry. HA has been identified as a good adsorbent material for environmental processes due to its specific structure that confers ionic exchange properties and adsorption affinity toward many pollutants. This biomaterial has already been applied for the removal of heavy-metal ions and organic compounds (phenols, dyes, etc.) from water [21,22]. Therefore, HA is a good candidate material for the development of MMMs as an alternative to the traditional porous ceramic membranes.

The major goal of this work was to prepare ultrafiltration MMMs and broadening the application of the HA in the field of water desalination. By taking the fact into account that no study has been previously carried out to prove the effect of addition of HA dispersed in acetone-dissolved 12-hydroxystearic acid (as surfactant) on the fabrication of the CA composite membranes, the present work focuses on the preparation and characterization of the CA–HA ultrafiltration MMMs using a modified-phase inversion method and on the removal of NaCl from aqueous solutions. The effects of the HA loading on the morphology, wettability, pure water flux (F), and solute rejection (R) of the resulting MMMs were investigated.

2. Experimental

2.1. Materials

$Ca(NO_3)_2{\cdot}4H_2O$, $(NH_4)_2HPO_4$, NH_4OH, CA polymer (M_r = 30,000, 83% acetyl groups), acetone, 12-hydroxystearic acid (HSA, $C_{18}H_{36}O_3$), NaCl and polyethylene glycol (PEG) with molecular weights of 600, 1,000, 1,500, 4,000, and 6,000 g/mol were purchased by Sigma-Aldrich (Germany). All chemicals were of analytical grade.

2.2. Hydroxyapatite nanopowder synthesis

The HA nanopowder was synthesized by wet chemical precipitation method based on our previous report, with some minor modifications [22]. Thus, an aqueous solution of 250 mL of $Ca(NO_3)_2{\cdot}4H_2O$ (0.01 M) was added dropwise to an appropriate amount of $(NH_4)_2HPO_4$ (0.01 M) aqueous solution to achieve predetermined Ca/P atomic ratio of 1.67. The solution was adjusted to pH 10.5 by adding small portions of NH_4OH (1 M). The suspension was matured for 3 h at approximately 60˚C under magnetic stirring. After that, the white powder was removed from the solution, washed with deionized water and dried at 110˚C for 24 h. The powder obtained was calcinated at 550˚C, in order to increase their crystallinity.

2.3. Hydroxyapatite nanopowder characterization

The phase composition of the HA powder was characterized by X-ray diffraction (XRD) with X'PERT PRO MRD diffractometer (PANalytical, the Netherlands) using monochromatic Cu Kα radiation (λ = 0.15418 nm). The average crystallite size (D) was calculated from XRD data by the Scherrer equation, using the peak at $2\theta = 25.9^\circ$ for (0 0 2) reflection. The morphology and chemical composition of the samples (sputtered with silver) were studied by scanning electron microscopy (SEM) coupled with energy dispersive X-ray spectroscopy (EDX) with QUANTA 200 3D microscope (FEI, the Netherlands). Particle size distributions, zeta potential, and point of zero charge of the HA sample were measured using dynamic light scattering (DLS) by a Zetasizer 3000 HS instrument (Malvern, UK). The wettability of the HA surface was estimated by measuring the contact angle with ultrapure water at ambient temperature by using a DataPhysics OCA-H200 goniometer (DataPhysics, Germany). The HA powder was pressed into pellets

(diameter 8.5 mm, width 3.5 mm) using an isostatic press. The pH measurements were realized with a Multi-Parameter Consort C831 (CONSORT, Belgium).

2.4. Membrane preparation

The pure CA membrane (denoted **CM**) was prepared by phase inversion method using CA polymer, acetone as solvent, 12-hydroxystearic acid (HAS) as amphiphilic surfactant and water as nonsolvent. The CA solution was made by dissolving 15 g of CA in 100 mL of 0.5% solution of HSA in acetone at atmospheric pressure and 30˚C for 4 h. The membrane was prepared by employing a two-step process. Firstly, the membrane with a thickness of about 800 μm was cast using a casting blade on a glass plate and was allowed to evaporate for 5 min in order to form the skin layer. Then, the cast film was subsequently immersed into a coagulation bath containing distilled water at 5 ± 1˚C for 20 min, to complete the phase separation, where exchange between the solvent (acetone) and the nonsolvent (distilled water) was induced. Finally, the membrane was dried in a vacuum oven at 60˚C for 24 h to remove residual solvents.

The CA–HA porous MMMs with variable HA contents were prepared by a modified-phase inversion method. The approach to prevent the agglomeration of the HA nanocrystals was to use the 12-hydroxystearic acid (HAS), an amphiphilic surfactant. The HA nanopowder was dispersed effectively in a 0.5% solution of HSA in acetone and then mixed homogeneously with the CA solution (15 wt.% CA dissolved in acetone) in order to produce a nanocomposite suspension. The weight percentages of HA loaded in each membrane were varied as stipulated in Table 1. The casting of the nanocomposite suspension and curing of the mixed matrix membranes were identical with those of the pure CA membrane. Series of flat sheet membranes with HA loading varying between 10 and 30 wt.% were made and the most performant samples were denoted CHM-10, CHM-20, and CHM-30 (Table 1). Above 30 wt.% HA, the membranes are brittle.

2.5. Membrane characterization

The morphology of the membranes was studied by SEM with QUANTA 200 3D microscope (FEI, the Netherlands). Fourier transform infrared (FTIR) spectroscopy was used to verify the HA incorporation in the CA matrix. Infrared spectra were collected in a FTIR DIGILAB SCIMITAR-SERIES spectrophotometer (Digilab, USA) using the attenuated total reflectance (ATR) technique. The scanning frequency range was 4,000–600 cm^{-1}. The overall porosity (ε) of the membranes was estimated by gravimetric method by the weight of liquid (here water) contained in the membrane pores, using the following equation:

$$\varepsilon = \frac{w_w - w_d}{\rho_w \cdot A \cdot l} \times 100 \quad (1)$$

where w_d is the weight of the dry membrane (g), w_w is the weight of the wet membrane after dipping into water for 2 h (g), ρ_w is the water density (0.998 g/cm^3) at room temperature, A is the effective area of the membrane (m^2), l is the membrane thickness (m).

Table 1
Characteristics of the unfilled and the HA-filled CA membranes

Sample	CM	CHM-10	CHM-20	CHM-30
HA content (wt.%)	0	10	20	30
Thickness[a] (μm)				
Membrane	401	389	367	352
Active layer	8.81	6.35	3.57	1.76
Effective pore radius in active layer[b] (nm)	3.38	2.76	2.39	2.12
Pore diameter in substructure[a] (μm)	63.23	51.82	42.69	36.76
MWCO (g/mol)[b]	2,591	2,103	1,976	1,932
Porosity (%)	58.9	63.5	66.3	70.1
Contact angle (˚)	69.4	53.1	46.3	44.5
Water uptake (%)	41.5	68.1	81.9	97.6
Pure water flux at 8 bar (L/m^2 h)	54.26	124.41	218.27	279.73
Salt rejection at 8 bar (%)	90.4	92.1	96.8	99.1

[a]By SEM method.
[b]Determined by PEG permeation tests. The results in the table are average values.

The surface hydrophilic behavior of the membranes was tested using water contact angle measurements and bulk hydrophilicity by water uptake study. Water contact angle measurements (five measures on different positions per sample, in triplicate, 2 mL drops of ultrapure water) have been carried out with a DataPhysics OCA-H200 goniometer (DataPhysics, Germany) and each measurement was considered to have ±2˚ accuracy. The water uptake was investigated by immersing the membrane strips (3×3 cm^2) in distilled water for 24 h at room temperature (25˚C) to ensure the membranes were fully saturated. Then, membranes were dried in a vacuum oven at 80˚C for 24 h and weighed. The water uptake (WU; %) of the membrane was calculated by means of the following relationship:

$$\mathrm{WU} = \frac{w_\mathrm{w} - w_\mathrm{d}}{w_\mathrm{d}} \times 100 \quad (2)$$

where w_d and w_w represent the weights of the dry and wet membranes, respectively (g).

2.6. Membrane performance

The performance of the membranes was studied by checking their pure water flux in order to determine the water transport behavior of the membranes. Then, the membranes were subjected to salt rejection study using 2,000 ppm NaCl feed solution with pH 9. Feed pH was adjusted by addition of 0.1 M NaOH. All permeation experiments were carried out in a homemade dead-end flow cell using circular membranes of 15 cm^2 effective area available for filtration. External pressure was applied using nitrogen cylinder capable of producing up to 12 bar pressure. Experiments were carried out at room temperature (25˚C) at diverse pressure (1–8 bar) during a single run using the same membrane sample. Three coupons from each membrane were evaluated to determine the pure water flux F (L/m^2 h) and solute rejection R (%) as follows:

$$F = \frac{V}{A \cdot t} \quad (3)$$

$$R = \left(1 - \frac{C_\mathrm{p}}{C_\mathrm{f}}\right) \times 100 \quad (4)$$

where V is volume of permeate collected (L), t is the sampling time (h), A is the membrane area (m^2), and C_p and C_f are the concentrations of the permeate and feed solutions determined by conductivity measurements using a conductivity meter (Multi-Parameter Consort C831, CONSORT, Belgium). The errors committed in concentration measurements and in flux and solute rejection determination were calculated, resulting in a relative error equal or lower than 0.8 L/m^2 h for flux and 3% for solute rejection.

The membranes after fouling were washed for 1 h at a low pressure of 5 bar with a dilute HCl solution. After cleaning, the membranes were rinsed with abundant amounts of deionized water. The cleanability of the membranes was characterized by comparison of the flux change before and after acid cleaning. After acid cleaning the water flux was almost completely restored to the initial flux.

The molecular weight cutoff (MWCO) of the obtained membranes was determined through permeation tests (at 8 bar) by using PEGs with various molecular weights as model solutes. The single compound solutions (with only one PEG) were prepared by dissolving weighed amount of PEG in salt-free distilled water at a concentration of 50 mg/L. The PEG concentrations in the feed and permeate were determined by gel permeation chromatography (GPC, Varian Company, USA). The MWCO value of the membrane corresponds to the molecular weight of the PEG that is 90% rejected by the membrane.

The effective pore radius (r_p, nm) of the obtained membranes was evaluated according to the Donnan steric partitioning pore model (DSP) developed by Richard Bowen and Mukhtar [23]. The rejections of neutral solute PEG with molecular weight of 1,000 g/mol (PEG1000, stokes radius $r_\mathrm{s} = 0.784$ nm) under different fluxes were measured by cross-flow permeation tests. During the filtration experiments, the applied pressure was changed between 0 and 10 bar. A laboratory cross-flow filtration apparatus was used in all experiments. The limiting observed PEG1000 rejection obtained from the rejection curve was taken as the limiting real rejection data (R_lim) and r_p was calculated by the equation [23]:

$$R_\mathrm{lim} = 1 - \left(1 + 0.054\lambda - 0.988\lambda^2 + 0.441\lambda^3\right)(1 - \lambda)^2 \quad (5)$$

where $\lambda = r_\mathrm{s}/r_\mathrm{p}$.

The main characteristics of the prepared membranes are summarized in Table 1.

3. Results and discussion

3.1. Hydroxyapatite characterization

To characterize the phase structure, crystallite size, morphology, and surface chemical composition of the HA sample, the XRD and SEM–EDX methods were

applied and the results are presented in Fig. 1. As evident in Fig. 1(a), the calcined HA powder shows the characteristic peaks in good agreement with the hexagonal hydroxyapatite phase (JCPDS Data Card 09-0432). The XRD peaks are well defined indicating a well-crystallized sample. The average crystallite size calculated by Scherrer equation from XRD line broadening was of 36.9 nm.

SEM image (Fig. 1(b)) provided evidence that HA was made up of nanocrystals. Some aggregates of individual crystallites were observed, being probably formed by the coalescence of the crystals or by direct initiation at the contacting surfaces. The measurements by DLS indicated that the individual nanometric particles (with an average size of about 40 nm) in percentage of about 81.3% predominate over the particle agglomerations (with an average size of about 250 nm). The EDX analysis confirms the presence of Ca, P, and O in HA crystallites (Fig. 1(c)). The Ca/P mole ratio was of 1.668 very close to 1.67 corresponding to the stoichiometric hydroxyapatite with the $Ca_{10}(PO_4)_6(OH)_2$ formula [24].

The HA surface is hydrophilic with an average contact angle of 42.48°. The zeta potential of the HA sample was of −17 ± 5 eV at pH of 7.6 and the point of zero charge (pH_{pzc}) was found at pH 7.4. The literature indicates the existence on the hydroxyapatite surface of the positively ($\equiv CaOH_2^+$) charged sites in acidic pH media or negatively ($\equiv OPO_3H^-$) charged sites in basic pH media [25]. Accordingly, hydrophilic and negatively or positively charged HA surfaces (depending on the pH of the medium) played an important role in enhancing the separation properties.

3.2. Membranes characterization

3.2.1. Membrane structure

It is well known that in order to obtain a ceramic–polymer composite with a micro- to nanoscale structure, a viscous polymer solution is usually mixed directly with ceramic powders or granules. In this connection, the problem related to the agglomeration of the ceramic particles is very important.

We aimed to solve the above problem and ultimately to apply this strategy to the obtaining of the asymmetric MMMs based on CA polymer and HA nanopowder. Thus, to prevent the agglomeration of the HA nanocrystals, a surfactant (12-hydroxystearic acid) was used. The HSA is a fatty acid containing a carboxylic head group coupled with a long hydrocarbon tail. It is well known that in nonaqueous solvents with low polarity, the carboxylic head group of fatty acids tends to adsorb onto the oxide nanoparticles [26,27].

Thus, in this study, the HA nanopowder was dispersed in acetone-dissolved 12-hydroxystearic acid and then mixed homogeneously with acetone-dissolved CA in order to produce a nanocomposite suspension. The dispersant is expected to be adsorbed on the inorganic particle surfaces and to provide steric barriers, preventing the HA agglomeration. The homogenous suspension was cast as a flat-sheet membrane under controlled conditions to produce asymmetric MMMs (as described in Membrane preparation section).

The asymmetric MMMs thus obtained were studied and characterized. The SEM micrographs of the CM and CHM-30 membranes are presented in Figs. 2 and 3.

As shown in the SEM images (Figs. 2(a) and 3(a)), all the membranes have asymmetric finger-like morphology consisting of a skin (top) layer, a support porous layer (substructure) and a bottom layer. Similar observations have been made by others authors for CA-inorganic membranes [28]. The membranes showed finger-like pores linked by sponge walls in the substructure. The walls contained a large numbers of pores that allowed the finger-like pores to

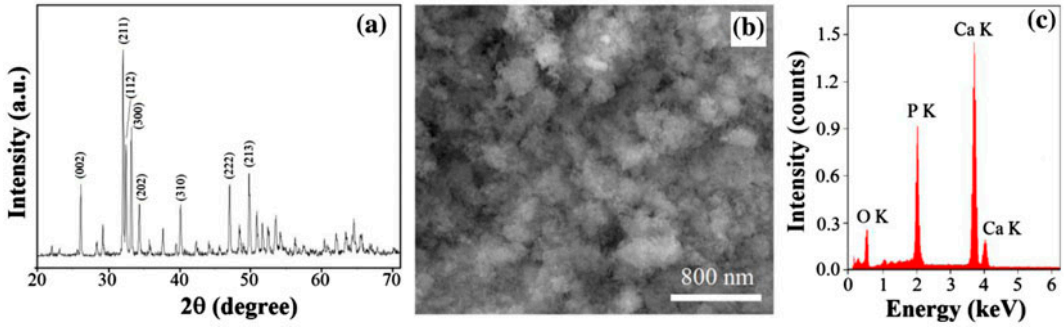

Fig. 1. HA nanopowder: (a) XRD pattern, (b) SEM image, and (c) EDX spectrum.

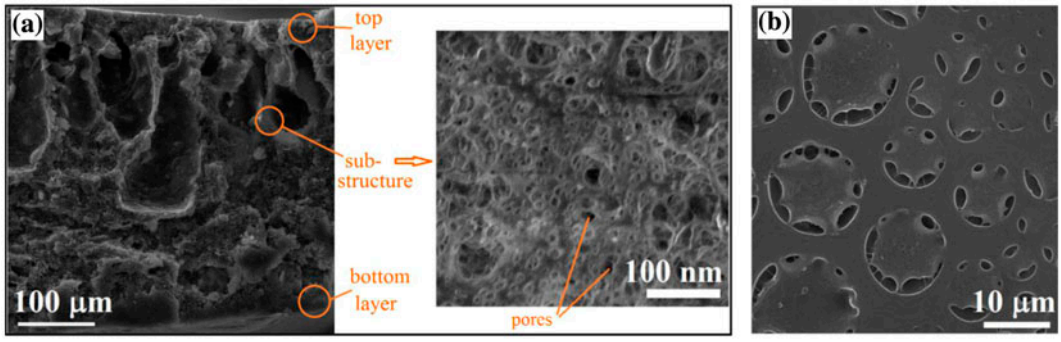

Fig. 2. SEM images of the CM membrane: (a) cross-section and (b) top surface.

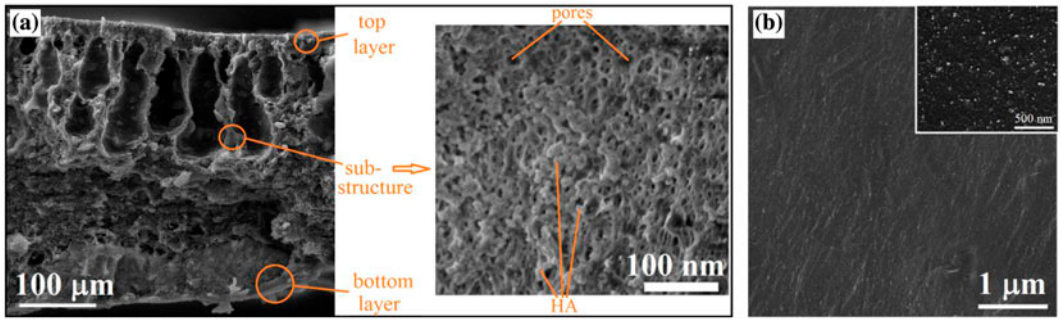

Fig. 3. SEM images of the CHM-30 membrane: (a) cross-section and (b) top surface (with an additional magnified image, scale bar 500 nm).

communicate with each other. In the case of MMMs with these open-pore arrangements, an easy accessibility of foreign ions or molecules able to interact with immobilized active sites of HA is expected.

The SEM images (Figs. 2(a) and 3(a)) also indicated that the membranes have an active (skin) layer of about several micrometers in thickness. The skin layer was found to possess ultrafine pores with diameters much smaller than those of the supported layer (Table 1). The SEM images at high magnification of the cross section confirmed a good incorporation of the HA into the CA polymer matrix. The most HA particles were dispersed uniformly enough within the membrane substructure (Fig. 3(a), inset).

The top surface of the CM sample (Fig. 2(b)) has a smooth structure with the presence of circular voids of diameters of the order of several micrometers (4–14 µm). In the case of the MMMs, these voids decreased in size and number, and even disappear, with increasing HA loading (Fig. 3(b)).

Addition of the HA nanopowder dispersed in a acetone with a small amount of 12-hydroxystearic acid to the CA casting solution affects the MMMs structure, namely a decrease in the skin thickness and in its pore size and an increase porosity of the composite membranes (Table 1). These modifications could be explained as follows. It is know that the fatty acids can affect the structure and the performances of the CA nanofiltration membranes [20]. During the phase inversion preparation process of hydrophilic CA membrane, the diffusion of solvent and nonsolvent is much slower than that of hydrophobic membranes. This leads to increase in the polymer concentration on the surface of the casted film resulting in a dense and thick skin layer, which leads to a low flux of the CA membranes. The addition of the additives of amphiphilic properties into the casting solution affects the penetration rate of the coagulant (water) in the phase inversion technique and therefore the structure of the prepared membrane and its performance [20]. These modification can be also explained by the interfacial interactions between the CA matrix and the HA filler. In the MMMs, it was possible that hydrogen-bonding interactions occurred between the polar groups of CA and the surface P-OH groups of HA; this was supported by the results of the FTIR analysis.

3.2.2. FTIR

The FTIR-ATR spectra of the pure HA powder and CA membrane were compared to those of the MMMs. The FTIR spectrum of the HA nanoparticles (Fig. 4(a)) showed adsorption bands around 568, 604, 1,036, and 1,101 cm^{-1} and corresponded to the phosphate (PO_4^{3-}) polyhedrons in the HA structure. The 3,672 cm^{-1} band was assigned to the surface P–OH groups, the peak at 3,564 cm^{-1} to the stretching vibrations of the lattice OH^- ions and the peak at 641 cm^{-1} to the O–H deformation mode. The broader band at 3,452 cm^{-1} was attributed to the water molecules adsorbed on the surface of HA.

The characteristic bands of CA membrane shown in Fig. 4(b) are attributable to the stretching vibration of the O–H (3,200–3,700 cm^{-1}), C–H (2,897 cm^{-1}), C=O (1,726 cm^{-1}), C–O of ester (1,329 and 1,193 cm^{-1}), and C–O of ether (1,021 cm^{-1}) groups.

The FTIR spectrum of the CHM-30 membrane depicted in Fig. 4(c) is indicative of the presence of the characteristic absorption peaks of both HA and CA. The hydrogen bonds between the O–H groups of the CA polymer and P–OH groups of HA were made evident by the presence of a broad band at 3,300–3,500 cm^{-1}. Apart from this, the FTIR spectrum indicates that the intensity of the IR bands related to C=O and O–H groups of CA increased by the addition of surfactant due to the presence of these groups of fatty acid molecules, which might be considered as a reason of fatty acid remaining in the casted membrane structure after the obtaining process.

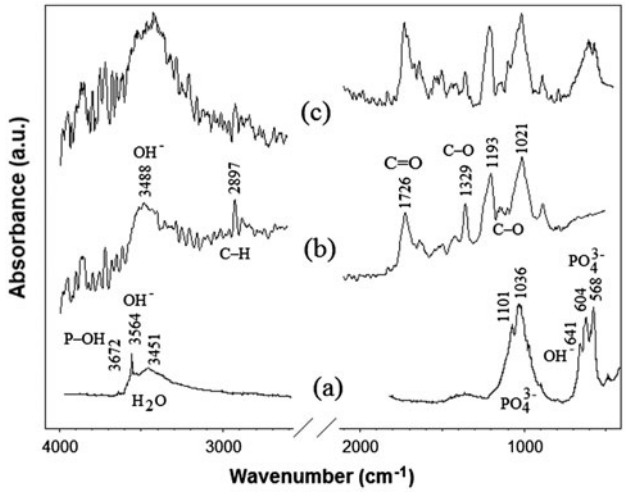

Fig. 4. The FTIR-ATR spectra of the HA powder (a), CM (b) and CHM-30 (c) membranes.

3.2.3. Water contact angle and water absorption

To investigate the effect of addition of HA and HAS on the hydrophilicity of the membranes, the water contact angle and water uptake of the membranes were measured and the obtained values presented in Table 1. The water contact angle decreased from about 59.4° to 44.5° with HA loading increasing from 0 to 30 wt.% which is indicative of an increased surface wettability because of the polar groups of the HA hosted on the CA surface.

The water uptake increased as the HA loading increased in the CA matrix indicating thus an increase in the hydrophilic sites in the CA matrix and an increase in the affinity of the membrane toward water. The HA surface contains hydrophilic sites which facilitated the uptake of water into the membrane matrix. Since the HA is a zwitterionic material, it could bind water molecules more strongly than other hydrophilic materials via electrostatically induced hydration [29]. Table 1 shows also that the HA loading resulted in an increase in the membrane porosity. This was why the MMMs could accommodate more water molecules increasing thus the overall uptake capacity.

These results indicate that the hydrophilicity of the MMMs was significantly improved by HA addition compared with CA membrane.

3.2.4. Membrane performances

The separation performances of the prepared membranes were described in terms of the water flux and salt rejection, and the results are summarized in Table 1 and Fig. 5. According to Fig. 5(a), the flux increased linearly with increasing applied pressure for all the membranes. The increase in HA concentration increases the water flux since a greater number of nanopores are formed. Consequently, these membranes are stable in producing the flux and suitable for further applications. As can be seen in Fig. 5(b), an increase in the NaCl rejection with increasing applied pressure is produced. All the prepared membranes showed a high salt rejection which was more than 90% at 8 bar of pressure (Table 1). The rejection capability of the prepared MMMs was higher than that of the unfilled CA membrane because the membrane surface was negative in nature. Hence, the Donnan exclusion principle played a significant role in governing the rejection of charged inorganic solutes.

The results indicate an improvement of the overall membrane performance. The best performing composite membrane, the CHM-30 sample, shows a retention of 99.1% and a high water permeability (34.96 L/m^2 h bar).

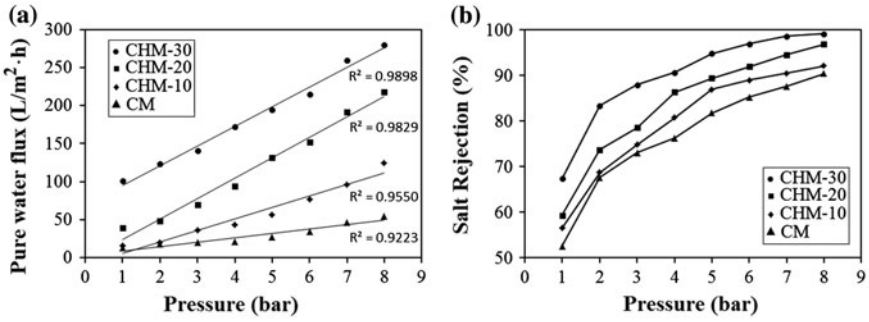

Fig. 5. Effect of the pressure on (a) flux and (b) NaCl rejection for the prepared membranes at 25°C and after 60 min of filtration (R^2 is the correlation coefficient). Errors in calculated flux and rejection are less than 0.8 L/m^2 h and 3%, respectively.

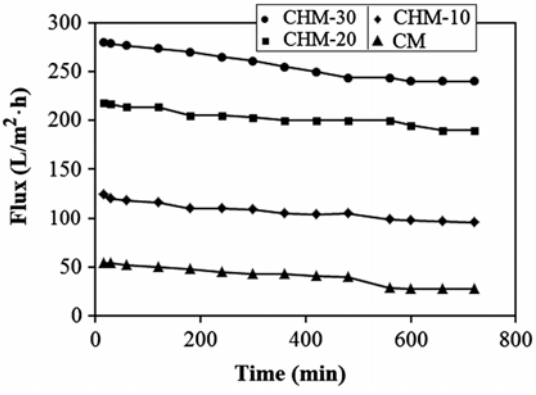

Fig. 6. Permeate flux over time for the prepared membranes at 25°C and 8 bar with a 2,000 ppm NaCl feed solution (pH 9). Errors in calculated flux are less than 0.8 L/m^2 h.

These results are probably due to the fact that the hydrophilicity of the composite membranes was improved by the HA addition. Consequently, many hydrophilic pores of nanometer sizes in the thin-film layer and pore walls of the MMMs could be produced. The MMMs showed a significant improvement in water flux performance (and water permeance) compared to CA membrane. This might have been caused by the incorporation of the HA phase showing a hydrophilic nature, surface charge (negatively or positively charged surface, depending on the pH of the medium), molecular sieve effect and larger resistance to swelling.

The fouling behavior of the membranes was also studied. Fig. 6 shows the permeation flux to decline with increasing filtration time, a period at a steady value being then noticed. This could be explained by membrane fouling.

The flux decline was no more than 15% for the composite membranes; the lowest value was of 14.21% for the CHM-30 sample in comparison with 49.31% for the CA membrane (CM sample). This result may be related to the membrane surface characteristics such as hydrophilicity, surface charge, surface roughness and pore structure, induced by increasing the concentration of HA.

The obtained results in this work demonstrate that the presence of the HA particles in the CA membranes improved the membrane performance in terms of their flux and fouling resistance.

4. Conclusions

The CA-nanoHA porous MMMs with variable HA contents were prepared by a modified phase inversion method. To prevent the agglomeration of the HA nanocrystals and to improve the performance of CA membranes, the HA nanocrystals were dispersed through the 12-hydroxystearic acid surfactant mediation within the CA matrix. Such addition resulted in the membranes with thinner active layer. The MMMs shown considerably higher pure water flux and permeation compared to CA membrane. A high retention of 99.1% and a high water permeability (34.96 L/m^2 h bar) were obtained by MMM with 30% HA loading. The incorporation of HA nanoparticles onto the CA matrix significantly enhanced the membrane's resistance to fouling with improved in the flux and the salt rejection.

References

[1] M. Ulbricht, Advanced functional polymer membranes, Polymer 47 (2006) 2217–2262.
[2] S. Pandey, S. Mishra, Sol–gel derived organic–inorganic hybrid materials: synthesis, characterizations and applications, J. Sol–Gel Sci. Technol. 59 (2011) 73–94.

[3] H. Vinh-Thang, S. Kaliaguine, Predictive models for mixed-matrix membrane performance: A review, Chem. Rev. 113 (2013) 4980–5028.
[4] J.R. Fried, Polymer Science and Technology, Prentice Hall, Upper Saddle River, NJ, 2003, pp. 315–317.
[5] E.M.V. Hoek, A.K. Ghosh, X. Huang, M. Liong, J. Zink, Physical–chemical properties, separation performance, and fouling resistance of mixed-matrix ultrafiltration membranes, Desalination 283 (2011) 89–99.
[6] G. Ciobanu, G. Carja, O. Ciobanu, Use of SAPO-5 zeolite-filled polyurethane membranes in wastewater treatment, Desalination 222 (2008) 197–201.
[7] G. Ciobanu, G. Carja, O. Ciobanu, Structure of mixed matrix membranes made with SAPO-5 zeolite in polyurethane matrix, Microporous Mesoporous Mater. 115 (2008) 61–66.
[8] J. Ahn, W.J. Chung, I. Pinnau, M. Guiver, Polysulfone/silica nanoparticle mixed-matrix membranes for gas separation, J. Membr. Sci. 314 (2008) 123–133.
[9] A.L. Ahmad, Z.A. Jawad, S.C. Low, S.H.S. Zein, A cellulose acetate/multi-walled carbon nanotube mixed matrix membrane for CO_2/N_2 separation, J. Membr. Sci. 451 (2014) 55–66.
[10] A.R. Moghadassi, Z. Rajabi, S.M. Hosseini, M. Mohammadi, Fabrication and modification of cellulose acetate based mixed matrix membrane: Gas separation and physical properties, J. Ind. Eng. Chem. 20 (2014) 1050–1060.
[11] R. Saranya, G. Arthanareeswaran, S. Sakthivelu, P. Manohar, Preparation and performance evaluation of nanokaolinite-particle-based polyacrylonitrile mixed-matrix membranes, Ind. Eng. Chem. Res. 51 (2012) 4942–4951.
[12] P. Sysel, E. Minko, M. Hauf, K. Friess, V. Hynek, O. Vopicka, K. Pilnacek, M. Sipek, Mixed matrix membranes based on hyperbranched polyimide and mesoporous silica for gas separation, Desalin. Water Treat. 34 (2011) 211–215.
[13] M. Sivakumar, A.K. Mohanasundaram, D. Mohan, K. Balu, R. Rangarajan, Modification of cellulose acetate: Its characterization and application as an ultrafiltration membrane, J. Appl. Polym. Sci. 67 (1998) 1939–1946.
[14] A.C. Puleo, D.R. Paul, S.S. Kelley, The effect of degree of acetylation on gas sorption and transport behavior in cellulose acetate, J. Membr. Sci. 47 (1989) 301–332.
[15] S.A. Ahmed, M.H. Sorour, H.A. Talaat, S.S. Ali, Functional analysis of cellulose acetate flat membranes prepared via casting technique, Desalin. Water Treat. 21 (2010) 115–121.
[16] X.R. Zhang, L.Z. Zhang, H.M. Liu, L.X. Pei, One-step fabrication and analysis of an asymmetric cellulose acetate membrane for heat and moisture recovery, J. Membr. Sci. 366 (2011) 158–165.
[17] R. Haddad, E. Ferjani, M.S. Roudesli, A. Deratani, Properties of cellulose acetate nanofiltration membranes. Application to brackish water desalination, Desalination 167 (2004) 403–409.
[18] G. Arthanareeswaran, P. Thanikaivelan, K. Srinivasn, D. Mohan, Synthesis, characterization and thermal studies on cellulose acetate membranes with additive, Eur. Polym. J. 40 (2004) 2153–2159.
[19] M. Sivakumar, D.R. Mohan, R. Rangarajan, Studies on cellulose acetate-polysulfone ultrafiltration membranes: II. Effect of additive concentration, J. Membr. Sci. 268 (2006) 208–219.
[20] N. Ghaemi, S. Madaeni, A. Alizadeh, H. Rajabi, P. Daraei, M. Falsafi, Effect of fatty acids on the structure and performance of cellulose acetate nanofiltration membranes in retention of nitroaromatic pesticides, Desalination 301 (2012) 26–41.
[21] N. Barka, K. Ouzaouit, M. Abdennouri, M. El Makhfouk, S. Qourzal, A. Assabbane, Y. Ait-Ichou, A. Nounah, Kinetics and equilibrium of cadmium removal from aqueous solutions by sorption onto synthesized hydroxyapatite, Desalin. Water Treat. 43 (2012) 8–16.
[22] G. Ciobanu, S. Ilisei, M. Harja, C. Luca, Removal of Reactive Blue 204 dye from aqueous solutions by adsorption onto nanohydroxyapatite, Sci. Adv. Mater. 5 (2013) 1–7.
[23] W. Richard Bowen, H. Mukhtar, Characterisation and prediction of separation performance of nanofiltration membranes, J. Membr. Sci. 112 (1996) 263–274.
[24] J.C. Elliott, Structure and Chemistry of the Apatites and Other Calcium Orthophosphates, Elsevier, Amsterdam, 1994.
[25] Å. Bengtsson, S. Sjöberg, Surface complexation and proton-promoted dissolution in aqueous apatite systems, Pure Appl. Chem. 81 (2009) 1569–1584.
[26] R.E. Johnson Jr., W.H. Morrison Jr., Ceramic powder dispersion in nonaqueous systems, in: G.L. Messing, K.S. Mazdiyasni, J.W. McCauley, R.A. Haber (Eds.), Advances in Ceramics. Ceramic Powder Science, vol. 95, American Ceramic Society, Westerville, 1987, pp. 323–348.
[27] H.W. Kim, H.H. Lee, J.C. Knowles, Electrospinning biomedical nanocomposite fibers of hydroxyapatite/poly(lactic acid) for bone regeneration, J. Biomed. Mater. Res. Part A 79A (2006) 643–649.
[28] G. Arthanareeswaran, T.K. Sriyamuna Devi, M. Raajenthiren, Effect of silica particles on cellulose acetate blend ultrafiltration membranes: Part I, Sep. Purif. Technol. 64 (2008) 38–47.
[29] S. Chen, L. Li, C. Zhao, J. Zheng, Surface hydration: Principles and applications toward low-fouling/nonfouling biomaterials, Polymer 51 (2010) 5283–5293.